SCEC Annual Meeting
September 14-17, 2020
Poster #110

Resolve 3-dimensional Deformation Field using GNSS and InSAR data

Zheng-Kang Shen[1], and Zhen Liu[2]

epartment of Earth, Planetary and Space Sciences, University of California, Los Angeles, CA 90095-1567

[2]Jet Propulsion Laboratory, California Institute of Technology, Pasadena, CA 91109

Summary

Three-dimensional (3-D) deformation field is essential in studying crustal deformation processes and natural hazards. We have recently developed an algorithm to integrate spatially limited GNSS and dimensionally limited InSAR data for a 3-D crustal deformation field at the Earth's surface (Shen and Liu, 2020). In the algorithm discrete GNSS data points are interpolated to a 3-D continuous velocity field, which is then combined with the InSAR line-of-sight (LOS) velocity data pixel by pixel using a least-squares method. Our method has the following advantages: 1) The GNSS data points are optimally interpolated through balancing a trade-off between spatial resolution and solution stability. 2) Realistic uncertainties for the interpolated GNSS velocity field are estimated using a newly developed algorithm and used as weights for GNSS data in GNSS-InSAR combination. 3) Realistic uncertainties for the InSAR LOS rate data are estimated and used as weights for InSAR data in the combination. 4) The algorithm has the flexibility in integrating InSAR data from multiple SAR sensors with different viewing geometries. 5) The ramps and/or offsets of the InSAR data are globally estimated for all the images to minimize data misfit, particularly at regions where the data overlaps. We have made initial efforts in applying this method to real data to restore 3-D velocity field in southern California. The GNSS velocity data we use is from the MEaSUREs project (http://geoapp03.ucsd.edu/gridsphere/gridsphere). We consider the InSAR data from different satellites such as the ERS-1,2 and Envisat from the 1990s-2000s, and more recent Sentinel-1A and 1B and L-band ALOS-2 ScanSAR data since 2015. Both Sentinel-1 and ALOS-2 data provide broad spatial coverage with good temporal coherence. The deformation field we obtained so far reveals water withdrawal induced subsidence and drought caused uplift at various regions in southern California.

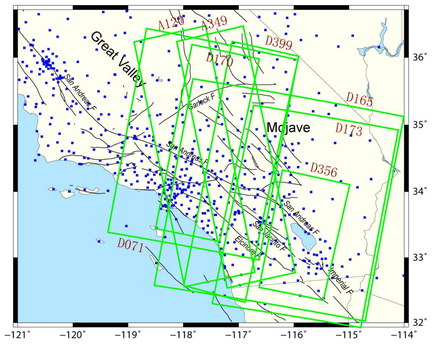

Figure 1. Study area in southern California. Black curves are active faults, blue squares are GNSS sites whose data are used in this study. The green frames denote the imprints of 8 InSAR tracks whose data are used in this study.

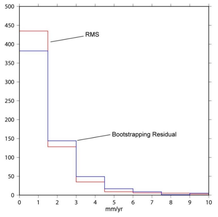

Figure 2. Histograms of GNSS velocity uncertainties. Blue curves are amplitudes of residual velocities from bootstrapping analysis, and red curves are uncertainties from GNSS velocity interpolation estimates.

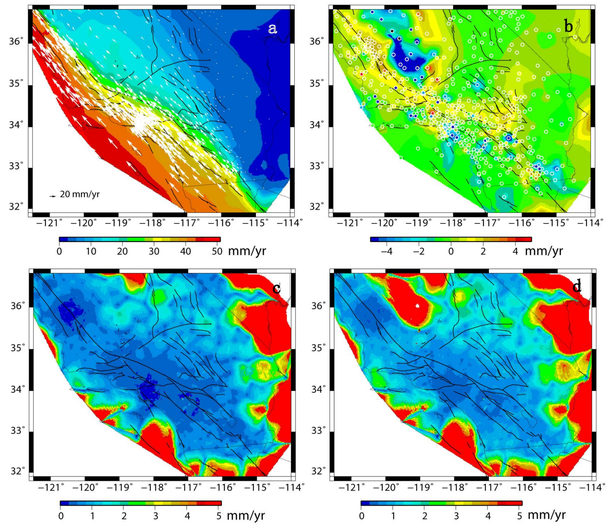

Figure 3. GNSS velocities and interpolation result. (a) White vectors are GNSS horizontal velocities in SNARF reference frame that are used in the combination with InSAR data. The background colors denote the amplitudes of interpolated horizontal velocity field. (b) Filled circles are GNSS vertical observations, and the background colors denote the interpolated vertical velocity field. (c) and (d) are uncertainties of east and up components of interpolated GNSS velocities, respectively.

1. GNSS data interpolation and uncertainty estimation

In our algorithm of GNSS and InSAR data integration, point-based discrete GNSS velocities are first interpolated to produce continuous 3-D vector map at chosen grids. The interpolation is based on an algorithm of Shen et al. (2015), which takes into account GNSS network density and configuration for data weighting. A Gaussian distance weighting function (w_d) and a Voronoi cell spatial weighting function (w_v) are used in the interpolation, which allow greater weighting for sites located closer to the chosen grid and/or occupying greater Voronoi cell areal space. The amount of weighting and degree of smoothing can be spatially variable and optimally determined based on *in situ* data strength, and are realized by assigning a common weighting parameter W for all the grid points: $W = \sum_{i=1}^{n\_k} w_d^i(k) * w_v^i(k)$. n_k is the number of neighboring data points used for the k^{th} grid point, $w_d^i(k) = \exp\left(-\frac{r_i^2}{\sigma_k^2}\right)$ is the Gaussian distance weighting function, r_i is the distance between the i-th GNSS site and the grid point, and σ_k is the smoothing distance constant. At each grid point σ_k is adjusted to meet W, which is a predetermined constant (W=3 for this study).

To combine the interpolated GNSS data with InSAR data, we need adequate estimates of GNSS velocity uncertainties from the interpolation, to be used as data weighting in the combination. Formal GNSS velocity uncertainties deduced in the interpolation process, however, are not fit for the job because they are largely determined by the amount of a priori information (i.e. the degree of smoothing) imposed during interpolation, which varies from grid to grid. It usually leads to apparently unreasonable results, that regions with sparser data points would have smaller uncertainty than regions with denser data points, and vice versa. To overcome the problem, we propagate errors from GNSS data input to interpolation output using the same interpolation functional form and least-square procedure as before, but keep σ_k as a constant σ_0 for all the region. In this way the same kind of a priori assignment algorithm will be applied for all the grids, and the only difference reflected in the output uncertainty estimates will be the in situ data strength. Parameter σ_0 is then determined through a statistical bootstrapping procedure, that velocity interpolation is performed at each GNSS site without utilization of the velocity datum of the site, and a differential velocity is evaluated for the site between the datum of the site and the interpolation value. We perform the bootstrapping analysis iteratively for all the sites with different assumptions of σ_0, and the optimal value of σ_0 (=17 km) is determined when the median of the amplitudes of 3-D residual velocities at the GNSS sites is equal to the median of the uncertainties from GNSS site velocity interpolation. **Fig. 2** plots histograms of the interpolated GNSS site velocity uncertainties and the bootstrapping velocity residuals with the optimal value of σ_0 incorporated, and the result shows an overall consistency of the two series.

2. InSAR data analysis, LOS rate, and uncertainty estimation

We processed the raw SAR data of ERS-1,2 and Envisat satellites from 1992 to 2010 for interferograms using a modified version of JPL/Caltech ROI_PAC software package. For Sentinel-1 TOPS and ALOS-2 ScanSAR data we use the InSAR Scientific Computing Environment (ISCE) software. General processing steps include interferometric phase flattening using precise orbit, topography phase correction, phase unwrapping, filtering and geocoding. For the ERS-2 data after 2001 that have Doppler issue due to gyroscope failure, we employ a maximum entropy approach to resolve Doppler ambiguity and identify all usable ERS-2 interferometric pairs. For Envisat ASAR sensors, we correct temporally correlated range ramp error due to long-term local oscillator frequency drift by adopting an empirical approach (Marinkovic and Larsen, 2013). For Sentinel-1 data, we use stack processor to co-register all SAR images to the same reference geometry and employ an enhanced spectral diversity technique to estimate azimuth misregistration between all SLC images in a stack sense. For L-band ALOS-2 data, we apply a range split-spectrum approach (Liang et al., 2017, 2018) to estimate ionosphere phase artifacts and correct them from the interferograms.

We use a variant of the Small Baseline Subset InSAR time series approach to solve for InSAR LOS time series and mean velocity (e.g., Sansosti et al., 2010). We incorporate topography dependent troposphere delay correction, residual DEM error and earthquake offset estimate, and employ spatiotemporal filtering to remove high frequency turbulent troposphere noise (Samsonov, 2010; Liu et al., 2014, 2019). For ERS and Envisat, since orbital ramp error for data from the same track is typically limited to a few acquisitions (e.g., Fattahi & Amelung, 2014) and small, we correct only affected interferograms through baseline re-estimation with the constraint of a priori GNSS based deformation model. The number of pairs with such correction is much less than the total number of interferograms that went into the analysis. This ensures that the influence of a priori model is negligible. Hundreds of interferograms that meet spatial and temporal baseline criteria are formed and used in the time series inversion. Table 1 lists SAR data and time span used in this study.

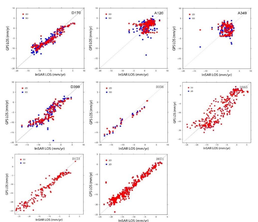

Figure 4. Comparison of InSAR and GNSS projected LOS data. Red and blue squares are projected 2-D (horizontal only) and 3-D components, respectively.

Table 1. SAR acquisitions and time span used in the study.

Track	Heading	Sensors	Time span
170	descending	ERS+Envisat	1992/06/17-2010/09/25
399	descending	Envisat	2003/06/30-2010/05/24
349	ascending	Envisat	2003/11/14-2010/10/08
120	ascending	Envisat	2003/10/29-2010/09/22
356	descending	ERS	1992/06/29-1999/10/15
165	descending	ALOS-2	2015/02/19-2019/12/05
173	descending	Sentinel-1	2014/11/10-2019/09/09
071	descending	Sentinel-1	2015/05/14-2019/07/04

The InSAR data are weighted by their LOS uncertainties. To characterize the uncertainties associated with InSAR deformation map, we adopt a Jackknife variance estimation approach [Efron and Stein, 1981], which provides a reasonable way to account for uncertainties arisen from lacking or missing dates, uncorrected residuals or other noises, and/or the influence of reference pixel and date. For each selected track of data we compute the differences between the LOS data input and the LOS values projected from GNSS velocities at pixels with GNSS occupation. We then determine a scaling factor based on the RMS of the LOS comparison (**Fig. 4**) and the statistically averaged LOS uncertainties and scale the data uncertainties accordingly.

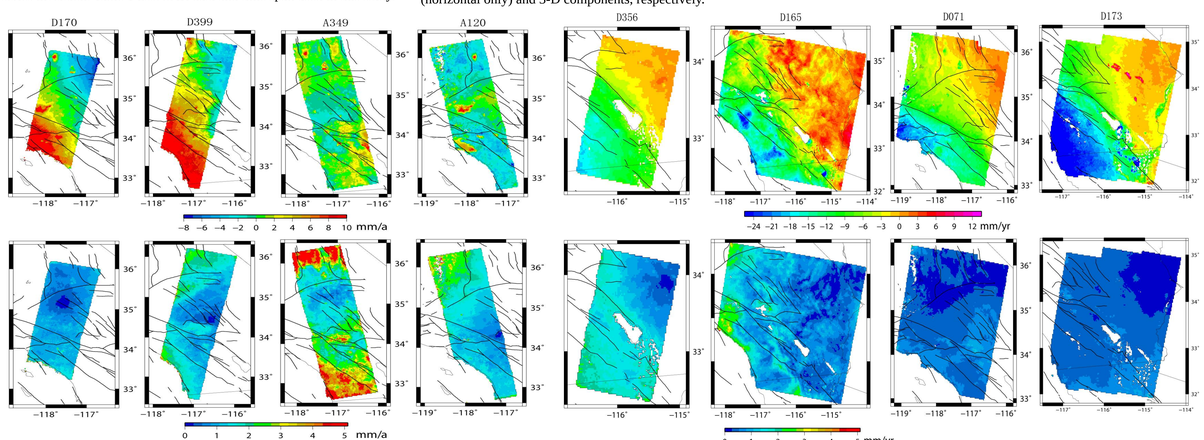

Figure 5. InSAR LOS rate data (top panel) and their uncertainties (lower panel).

3. GNSS and InSAR velocity data combination for Southern California

We first divide the region into rectangle grid cells (0.02 x0.02 deg). The coarse grid is used to reduce the computation cost. At each grid cell, all of the available InSAR LOS rate data from different tracks (with different viewing geometries) are used. For each of the LOS rate images all the pixel data within the grid cell are averaged to produce a mean rate, weighted by the uncertainties.

We then determine the offsets/ramps of InSAR images. These parameters are solved together with the 3-D deformation components, and some GNSS data and their interpolated values are included in the estimate to stabilize the inversion. Because these offset/ramp parameters are correlated with all the deformation parameters in the study area, an optimal estimate of the offsets/ramps means a global solution for all the parameters involved. To limit the scope of inversion We include only (a) the grid points containing direct GNSS velocity observations, and (b) decimated grid points (e.g. by a factor of 10 in each dimension). The global solution is obtained through the least-squares regression.

In the last step the components of offsets/ramps are removed from the InSAR LOS data, and the 3-D velocity is solved for each grid cell through least-squares regression, with GNSS interpolated velocity and all the LOS data for the cell incorporated. The rescaled GNSS and InSAR data uncertainties are used to weight the data input. The GNSS vertical data are not used to constrain the final solution, leaving the vertical deformation constrained entirely by InSAR data. .

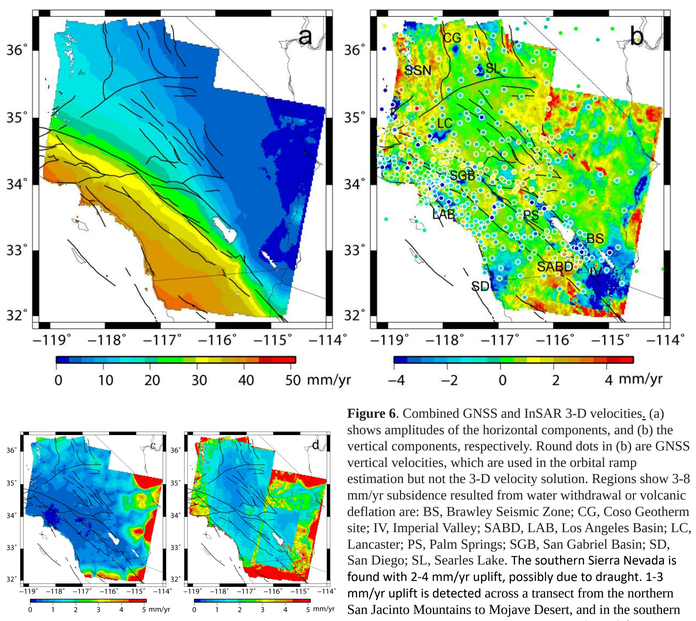

Figure 6. Combined GNSS and InSAR 3-D velocities. (a) shows amplitudes of the horizontal components, and (b) the vertical components, respectively. Round dots in (b) are GNSS vertical velocities, which are used in the orbital ramp estimation but not the 3-D velocity solution. Regions show 3-8 mm/yr subsidence resulted from water withdrawal or volcanic deflation are: BS, Brawley Seismic Zone; CG, Coso Geotherm site; IV, Imperial Valley; SABD, LAB, Los Angeles Basin; LC, Lancaster; PS, Palm Springs; SGB, San Gabriel Basin; SD, San Diego; SL, Searles Lake. The southern Sierra Nevada is found with 2-4 mm/yr uplift, possibly due to draught. 1-3 mm/yr uplift is detected across a transect from the northern San Jacinto Mountains to Mojave Desert, and in the southern Anza-Borrego Desert (SABD) region near the California-Mexico border. (c) and (d) are solution uncertainties for the east and vertical components respectively.

4. Conclusions

1. Using optimally estimated GNSS and InSAR uncertainties to weight the data provides proper accounting of the solution uncertainties, and helps adequately assess the solution quality and reliability.
2. GNSS networks are usually too sparse to adequately detect localized vertical deformation, particularly in regions affected by hydrologic processes. Existence of certain outliers in the dataset makes identification of localized deformation even more challenging. The optimal approach is therefore to use the GNSS vertical data to constrain the satellite orbital ramps only, and leave the localized vertical deformation solved by InSAR, aided by GNSS horizontal constraints.
3. The GNSS and InSAR data are generally consistent for the horizontal velocities at sub-millimeter per year level. The localized vertical deformation is detected, particularly for regions experiencing hydrologic and/or other tectonic/anthropogenic induced subsidence or uplift. These regions include the Los Angeles basin, San Gabriel basin, Lancaster, Palm Springs, Searles Lake, San Diego, Brawley Seismic Zone, and Imperial Valley where hydrologic and volcanic processes caused induced subsidence of up to 3-8 mm/yr. They also include the southern Sierra Nevada region which underwent drought related uplift of 2-3 mm/yr. Uplift of 1-3 mm/yr is detected across a transect from the northern San Jacinto Mountains to Mojave Desert, and in the southern end of the Anza-Borrego Desert region near the California-Mexico border.

Reference

Shen, Z. K., & Liu, Z. (2020). Integration of GPS and InSAR Data for Resolving 3-Dimensional Crustal Deformation. *Earth and Space Science*, *7*(4), e2019EA001036.